Evaluation of the porosity parameter for a perforated wall wind tunnel using measured wall pressure distributions

Mihaela BURGHIU (MANEA)*,[1,2], Adrian BURGHIU[1,2]

*Corresponding author
[1]INCAS – National Institute for Aerospace Research "Elie Carafoli",
B-dul Iuliu Maniu 220, Bucharest 061126, Romania,
manea.mihaela@incas.ro*, burghiu.adrian@incas.ro
[2]POLITEHNICA University Bucharest,
Splaiul Independentei 313, 060042, Bucharest, Romania

DOI: 10.13111/2066-8201.2022.14.3.1

Received: 03 June 2022/ Accepted: 11 July 2022/ Published: September 2022

Abstract: *The existing analytical methods for determining and correcting the effect of wind tunnel walls on experimental data are based on the hypothesis of potential flow. A useful simplification of the boundary conditions used to describe the perforated walls was to consider the wall as homogeneous, the solid and free portions not being treated separately, but as an equivalent permeable surface. The approximation of the wall behaviour during the experiment was possible by defining a porosity parameter. The purpose of this paper is to estimate the porosity parameter for the perforated walls of a trisonic wind tunnel by evaluating the pressure distributions measured on the walls of the test section.*

Key Words: *wind tunnel, wall pressure distributions, porosity parameter, perforated wall*

1. INTRODUCTION

Most methods used for determining wall corrections that use idealized boundary conditions are based on the potential flow hypothesis. Thereby, it is assumed that the flow in the tunnel is governed by the equation:

$$\frac{\partial^2 \varphi}{\partial x^2} + \frac{\partial^2 \varphi}{\partial y^2} + \frac{\partial^2 \varphi}{\partial z^2} = 0 \tag{1}$$

where φ is the disturbance velocity potential of the entire flow field, and is defined as the superposition of wall interference and model potentials.

$$\varphi = \varphi_M + \varphi_W \tag{2}$$

where φ_M is the model potential and φ_W is the interference potential.

The potential due to the model is considered to be a known solution of the above equation, and therefore the potential due to the walls can be determined if the boundary conditions at the wind tunnel walls are met.

Keller [1] generalized the boundary condition for the perforated walls and developed a panel method to determine the wall corrections. The boundary condition is defined as [1]:

$$c_1\varphi + c_2\frac{\partial\varphi}{\partial x} + c_3\frac{\partial\varphi}{\partial n} + c_4\frac{\partial^2\varphi}{\partial x\partial n} = 0 \tag{3}$$

where n is the direction normal to the wall.
The $c_1, .., c_4$ coefficients are described in Table 1:

Table 1: Keller's boundary condition coefficients [1]

Type of boundary condition	c_1	c_2	c_3	c_4
Closed wall	0	0	1	0
Open jet	0	1	0	0
Perforated wall	0	1	$\frac{1}{\mathrm{P}}$	0
Ideal slotted wall: integrated form	1	0	K	0
Ideal slotted wall: differentiated form	0	1	$\frac{\partial \mathrm{K}}{\partial x}$	K
Slotted wall including the viscosity in slots	0	1	$\frac{\partial \mathrm{K}}{\partial x} + \frac{1}{\mathrm{P}}$	K

where P is the porosity parameter and K is the slot parameter.

These boundary conditions describing the ideal perforated wall can be seen as first order approximations in the assessment of the wall crossflow characteristics. These analytical expressions aim to capture the primary character of the flow.

As stated by Vayssaire in [2] it is not possible to determine the porosity parameter using analytical methods, hence it must be determined by means of experimental techniques.

Moreover, there is no universal method which can describe the procedure used to determine the porosity parameter, therefore each facility conducts its own procedure in this assessment.

The purpose of this paper is to evaluate the porosity parameter for the perforated walls of the INCAS trisonic wind tunnel, by directly comparing the pressure distributions measured on the lower and upper walls of the test section with the pressure distributions generated using the potential flow hypothesis and a theoretical boundary condition.

2. COMPUTATION OF PRESSURE DISTRIBUTIONS

The pressure distributions are computed using the panel method presented in [1], [3].

The wind tunnel walls are represented by rectangular elements, defined by a constant strength source distribution over each element.

The model lifting effect is represented by using discrete horseshoe vortices distributed along the quarter chord line; the load distribution is assumed to be elliptic [4]. The vortex strength is the area under the load distribution curve. The blockage effect is described by using a distribution of three dimensional doublets.

If φ^* is the velocity potential of an rectangular element divided by the source strength [1], [5], then

$$\varphi_{\mathrm{W}} = \sum_{i=1}^{\mathrm{N}} \varphi_i^* \sigma_j' \tag{4}$$

where σ' is the source strength.

The boundary conditions for each of the four walls are defined as:

$$\frac{\partial \varphi}{\partial x} - \frac{1}{P}\frac{\partial \varphi}{\partial z} = 0 \tag{5}$$

$$\frac{\partial \varphi}{\partial x} + \frac{1}{P}\frac{\partial \varphi}{\partial z} = 0 \tag{6}$$

for the top and bottom walls, and

$$\frac{\partial \varphi}{\partial x} - \frac{1}{P}\frac{\partial \varphi}{\partial y} = 0 \tag{7}$$

$$\frac{\partial \varphi}{\partial x} + \frac{1}{P}\frac{\partial \varphi}{\partial y} = 0 \tag{8}$$

for the side walls. The boundary conditions are satisfied at the centroid of each element.

To compute the source strength it is necessary to solve a matrix equation for the values of σ_j'. If the test section is represented by N panels, the above equation can be written at the centroid of each rectangular element as [6]:

$$\begin{aligned}\sum_{j=1}^{N}\left[c_1(i)\varphi_{i,j}^{*} + c_{2(i)}\left(\frac{\partial \varphi^{*}}{\partial x}\right)_{i,j} + c_3(i)\left(\frac{\partial \varphi^{*}}{\partial n}\right)_{i,j} + c_4(i)\left(\frac{\partial \varphi^{*}}{\partial x \partial n}\right)_{i,j}\right]\cdot \sigma_j' \\ = -\left(c_1(i)\varphi_{M,i} + c_{2(i)}\left(\frac{\partial \varphi_M}{\partial x}\right)_i + c_3(i)\left(\frac{\partial \varphi_M}{\partial n}\right)_i \right. \\ \left. + c_4(i)\left(\frac{\partial \varphi_M}{\partial x \partial n}\right)_i\right)\end{aligned} \tag{9}$$

The resulting linear system can be written in matrix form:

$$\begin{bmatrix} A_{1,1} & \dots & A_{1,j} & \dots & A_{1,N} \\ \vdots & \vdots & \vdots & \vdots & \vdots \\ A_{i,1} & \dots & A_{i,j} & \dots & A_{i,N} \\ \vdots & \vdots & \vdots & \vdots & \vdots \\ A_{N,1} & \dots & A_{N,j} & \dots & A_{N,N} \end{bmatrix}\begin{bmatrix} \sigma_1' \\ \vdots \\ \sigma_j' \\ \vdots \\ \sigma_N' \end{bmatrix} = \begin{bmatrix} B_1 \\ \vdots \\ B_i \\ \vdots \\ B_N \end{bmatrix} \tag{10}$$

The values obtained by solving the above equation are then used for the computation of the pressure distributions on the wind tunnels walls. The pressure coefficient at a wall panel centroid can be determined using:

$$C_p(i) = -2\frac{u(i)}{U_\infty} = \frac{-2}{U_\infty}\left[\left(\frac{\partial \varphi_M}{\partial x}\right)_i + \sum_{j=1}^{N}\left(\frac{\partial \varphi^{*}}{\partial x}\right)_{i,j}\sigma_j'\right] \tag{11}$$

For any flow field point, k, the perturbation velocity component can be written as:

$$u_W(k) = \left(\frac{\partial \varphi_W}{\partial x}\right)_k = \sum_{j=1}^{N}\left(\frac{\partial \varphi^{*}}{\partial x}\right)_{k,j}\sigma_j' \tag{12}$$

For higher subsonic Mach numbers, the Prandtl-Glauert compressibility factor needs to be applied for the potential equation and the boundary conditions.

Hence, the governing equation becomes:

$$\beta^2 \frac{\partial^2 \varphi}{\partial x^2} + \frac{\partial^2 \varphi}{\partial y^2} + \frac{\partial^2 \varphi}{\partial z^2} = 0 \tag{13}$$

where

$$\beta = \sqrt{1 - M^2} \tag{14}$$

3. WALL PRESSURE DISTRIBUTION MEASUREMENT

The wall pressure measurements were performed in the INCAS trisonic wind tunnel by using two tubular pressure probes. The model which was used during the experiments was ONERA M4R. The 1.2 m x 1.2 m trisonic wind tunnel is of the blowdown type with a speed range from low subsonic to a maximum supersonic Mach number of 3.5.

This range includes transonic Mach numbers which are obtained by using a perforated wall transonic test section [7]. The transonic section is a cylindrical pressure shell of approximately 4 m in length which contains the perforated wall test section, surrounded by the plenum chamber. The perforations have a 10 mm diameter and they are inclined at 60^o. The porosity of the walls may be adjusted at values continuously varying between 0.35% and 9.1% by means of pairs of perforated plates.

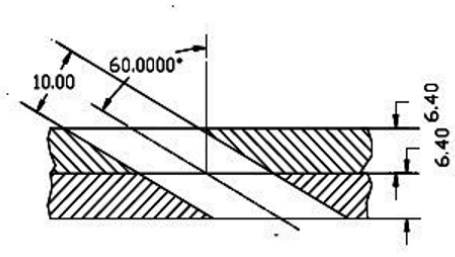

Fig. 1 – INCAS perforated wall test section maximum porosity

Fig. 2 – INCAS perforated wall test section

ONERA M4R has a typical transonic transport configuration and is part of ONERA calibration models family.

The main dimensions for ONERA M4R model are presented in Table 2 [8]. The wings have a 30^o sweep, a taper ratio of 0.3 and a 7.31 aspect ratio and. Wing and tail air foils have a 'peaky' type symmetric cross section [9].

Table 2: ONERA models characteristics

Model	**M1**	**M2**	**M3**	**M4R**	**M5**
Wingspan, b [m]	0.2868	0.369	0.474	0.635	0.982
Mean aerodynamic chord $\bar{c}$, [m]	0.040	0.052	0.066	0.0889	0.137
Wing area, S [m^2]	0.011	0.019	0.031	0.05516	0.132
Fuselage length, L [m]	0.309	0.397	0.511	0.684	0.764
Fuselage diameter, D [m]	0.036	0.047	0.060	.08033	0.0897

Fig. 3 – ONERA M4R model

The pressure distribution measurements on the walls of the transonic test section were performed using two tubular probes, located on the top and bottom walls.

Fig. 4 – Tubular pressure probes placed on the top and bottom walls of the test section

Fig. 5 – The tip of the pressure probes

The tip of the probe has the shape of a cone with a semi-angle of 10°. The tip is followed by a cylinder with a 28 mm diameter and 400 mm apparent length.

The body of the probe is fixed on the downstream portion of the insertion wall using two mounting brackets and M6 screws. Because the perforated plate, together with the probe, moves according to porosity variation, the tip must be installed in various positions.

Hence, the mounting brackets for the tip are each equipped with a slot which allows a maximum axial movement of 18 mm.

The body includes a pipe with 28 mm diameter and 3200 mm length and is fixed on the insertion wall using 14 mounting brackets and M4 screws. Each probe has 44 pressure taps from which 32 were used to measure the pressure distributions.

The pressures were measured using two electronic pressure scanning modules, with a measuring capacity of ± 25 psid. The pressure coefficients were computed using:

$$C_p = \frac{p - p_s}{q} \tag{15}$$

$$q = \frac{\gamma}{2} p_s M^2 \tag{16}$$

where p_s is the measured static pressure, p is the measured pressure, q is the dynamic pressure, γ is specific heat ratio and M is the Mach number.

4. RESULTS

The computation of the pressure distributions was performed for 0.5 and 0.85 Mach numbers and for a porosity parameter that described several porosity cases. Also, computations were performed for the solid wall case, when the coefficients defined by Keller [1], c_2 and c_3 have the values 0 and 1, respectively, and also for the open jet case, when $c_2 = 1$ and $c_3 = 0$.

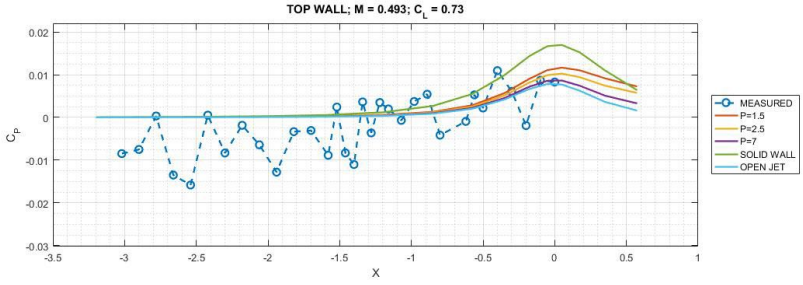

Fig. 6 – Measured and computed wall pressure distributions for M=0.5, top wall

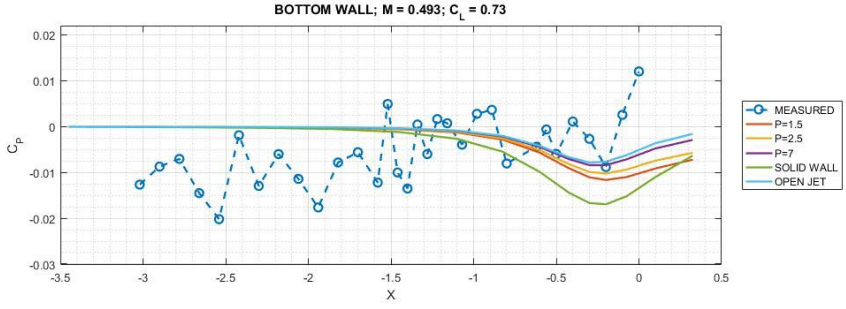

Fig. 7 – Measured and computed wall pressure distributions for M=0.5, bottom wall

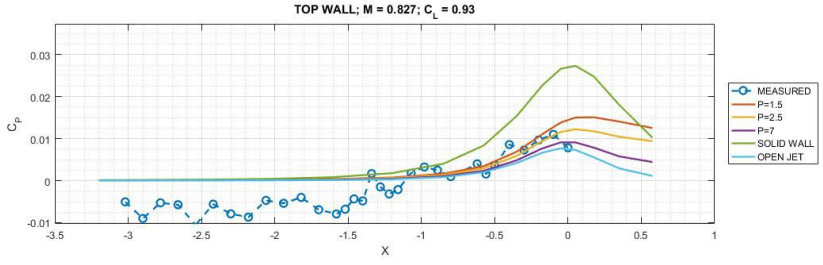

Fig. 8 – Measured and computed wall pressure distributions for M=0.83, top wall

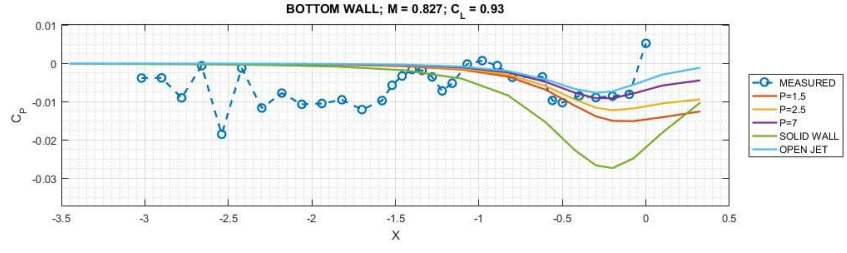

Fig. 9 – Measured and computed wall pressure distributions for M=0.83, bottom wall

Fig. 6 and Fig. 8 present the measured versus the computed pressure distributions on the top wall of the test section at M=0.5 and M=0.83. The computations were performed for three values of the porosity parameter ($P = 1.5, P = 2.5, P = 7$) and also for the open jet and solid wall cases. The same cases are presented in Fig. 7 and Fig. 9 for the bottom walls.

As it can be observed, the porosity parameter value at which the calculated distributions seem to fit better the measurements in all cases, is situated around 2.5.

For the bottom wall at M=0.83, this value seems however to be a bit high. This may suggest that the use of different porosity parameter is needed, as stated in [10], which shows that good agreement between theoretical and experimental wall pressure distributions is met only after introducing two porosity parameters describing the floor and the ceiling, respectively. However, due to the measured pressures scattering degree, a detailed analysis on the use of different porosity parameters is currently not possible. Nevertheless, the use of a 2.5 porosity parameter in assessing the lift interference for the INCAS trisonic wind tunnel and ONERA M4R model at M=0.5 leads to acceptable results [3].

5. CONCLUDING REMARKS

The nature of the wind tunnel flow near the test section walls may be evaluated from local pressure measurements. In this paper, a comparison between experimental pressure measurements and computed pressure distributions was performed. The classical theory used for pressure computation uses a linear characteristics description of the walls in which the velocity normal to the wall is proportional to the pressure drop across the wall.

A comparison between the measured and theoretical pressure distributions for the INCAS Trisonic wind tunnel and ONERA M4R model was made, and it was concluded that the value of the porosity parameter has the approximate value of 2.5.

The wall pressure distributions measurements provide important information regarding the flow in the perforated wall test section and, as a consequence, the wall corrections can be computed with a greater degree of accuracy.

REFERENCES

[1] J. D. Keller, *Numerical Calculation of Boundary-Induced Interference in Slotted or Perforated Wind Tunnels Including Viscous Effects in Slots*, Langley Research Center, Hampton, 1972.

[2] J. C. Vayssaire, *Survey of Methods for Correcting Wall Constraints in Transonic Wind Tunnels*, AGARD R-601, April 1973.

[3] M. Manea, A. Burghiu, Lift Interference in Wind Tunnels with Perforated and Solid Walls, *INCAS BULLETIN*, (print) ISSN 2066–8201, (online) ISSN 2247–4528, ISSN–L 2066–8201, vol. 13, issue 1, pp. 105-111, 2021, https://doi.org/10.13111/2066-8201.2021.13.1.11

[4] M. Mokry and R. Galway, *Analysis of Wall Interference Effects on ONERA Calibration Models in the NAE 5-ft. Wind Tunnel*, NRC Aeronautical Report, Ottawa, 1977.

[5] J. D. Keller, R. H. Wright, *A Numerical Method of Calculating the Boundary-Induced Interference in Slotted or Perforated Wind Tunnels of Rectangular Cross Section*, Langley Research Center, Hampton, 1971.

[6] N. Ulbrich, *Description of Panel Method Code ANTARES*, Ames Research Center, California, 2000.

[7] F. Munteanu, INCAS Trisonic Wind Tunnel, *INCAS BULLETIN*, (print) ISSN 2066–8201, (online) ISSN 2247–4528, ISSN–L 2066–8201, vol. 1, no. 1, 5-11, 2009, http://dx.doi.org/10.13111/2066-8201.2009.1.1.2

[8] F. Munteanu, *Experiments with ONERA M4R*, INCAS Internal Report, Bucharest, 2012.

[9] T. W. Binion, *Tests of the Onera Calibration Models in Three Transonic Wind Tunnels*, AEDC, Tennessee, 1976.

[10] M. Mokry, D. J. Peake, A. J. Bowker, *Wall Interference on Two-Dimensional Supercritical Airfoils, Using Wall Pressure Measurements to Determine the Porosity Factors for Tunnel Floor and Ceiling*, National Research Council, Ottawa, 1974.